Can. J. Remote Sensing, Vol. 30, No. 2, pp. 150–156, 2004

Research Note / Note de recherche

Spectral emissivity of northern land cover types derived with MODIS and ASTER sensors in MWIR and LWIR

Véronique Payan and Alain Royer

Abstract. The purpose of this study is to evaluate the potential of satellite-derived emissivity in middle-wave infrared (MWIR) and long-wave infrared (LWIR) for land surface characterization. We compared emissivities derived from advanced spaceborne thermal emission and reflection radiometer (ASTER; temperature emissivity separation (TES) algorithm; validated data V003) and moderate resolution imaging spectroradiometer (MODIS; two different algorithms, classification-based emissivity method and day–night land surface temperature algorithm; provisional data V003) images acquired over northern Canadian regions. We observed disparities in emissivity dynamic range between each algorithm, and a bias also exists for the MODIS day–night algorithm (–0.02 versus ASTER). Lastly, we related MODIS and ASTER emissivity images with land cover type data derived from MODIS visible and near-infrared observations. Emissivity characteristics were determined for each class encountered. However, we generally observed a significant emissivity spatial heterogeneity inside a single land cover class.

Résumé. Cette étude vise à évaluer le potentiel de l'émissivité en infrarouge médian et thermique afin de caractériser les surfaces terrestres. Nous avons comparé les émissivités dérivées d'images ASTER (algorithme TES, données validées V003) et MODIS (2 algorithmes différents, Méthode basée sur la classification de l'émissivité et algorithme Jour–nuit, données non validées V003) acquises sur des régions nordiques canadiennes. Nous avons relevé des disparités entre les dynamiques des émissivités retrouvées par les algorithmes et un biais existe pour les émissivités évaluées par l'algorithme Jour–nuit de MODIS (–0,02 par rapport au données ASTER). Enfin, nous avons mis en relation les images d'émissivité MODIS et ASTER avec des données de couverture du sol, aussi dérivées d'observations MODIS. Des valeurs moyennes d'émissivité pour les classes présentes ont été déterminées. Mais nous observons en général une hétérogénéité spatiale significative pour l'émissivité à l'intérieur d'une même classe de couverture du sol.

Introduction

Emissivity determination on northern land cover types in the infrared spectral region (middle-wave infrared (MWIR, 3.4–5.2 μm) and long-wave infrared (LWIR, 7.5–14.0 μm)) is of particular interest. In fact, emissivity has an important impact on the determination of surface net heat flux, as the thermal radiation of a surface is the product of its emissivity and temperature. Several methods exist to extract spectral parameter emissivity and temperature, and a good review of these is given by Dash et al. (2002). Also, there are indications that global climate changes could have strong effects in these northern areas, on permafrost for example (Smith and Burgess, 1999).

New spaceborne sensors such as the moderate resolution imaging spectroradiometer (MODIS) (Justice et al., 1998) and the advanced spaceborne thermal emission and reflection radiometer (ASTER) (Yamaguchi et al., 1998) on the National Aeronautics and Space Administration (NASA) Earth Observing System TERRA[2] satellite, launched in December 1999, provide for the first time infrared emissivity imaging coverage over large spatial regions.

In this paper, we present a preliminary overview of MODIS and ASTER emissivity products derived from different emissivity–temperature separation methods. We present the data and method used for this study, compare the different emissivity–temperature extraction methods, and relate MODIS and ASTER emissivity images with land cover data, also derived from MODIS, determining emissivity values for each class encountered.

Data and methodology

Study zones

Northern Canadian regions are particularly interesting as latitudinal vegetation density gradients are clearly present. The three standard MODIS tiles considered are geographically located in **Figure 1**. About 10 dates during the summer of 2001

Received 9 July 2003. Accepted 12 November 2003.

V. Payan and A. Royer.[1] Centre d'Applications et de Recherches en Télédétection, Université de Sherbrooke, Sherbrooke, QC J1K 2R1, Canada.

[1]Corresponding author (e-mail: alain.royer@usherbrooke.ca).

[2]MODIS is also on the NASA AQUA satellite launched in May 2002.

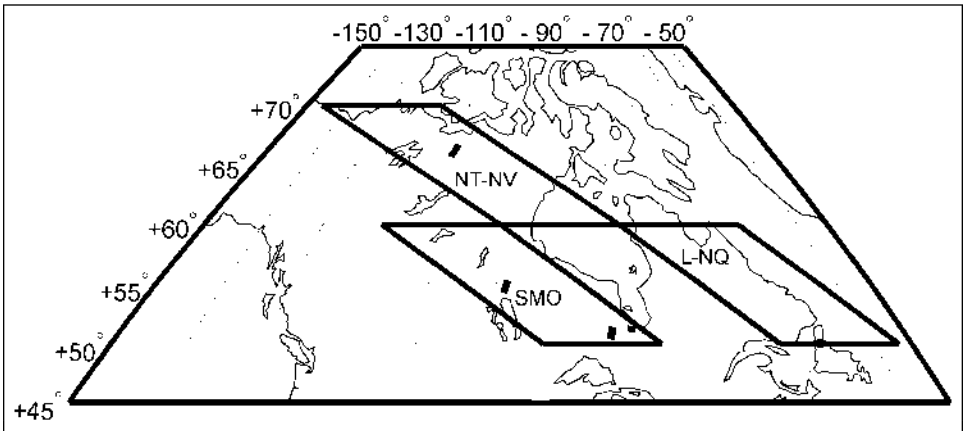

Figure 1. MODIS (large, open, diamond-shaped areas) and ASTER (small, solid symbols within the MODIS areas) image location over Canada. L–NQ, Labrador and northern Quebec; NT–NV, northern territories and Nunavut; SMO, Saskatchewan, Manitoba, and Ontario.

were selected for each tile. We searched for acquired ASTER images (**Figure 1**) corresponding to MODIS dates and locations, but only a few images were available (from two to six ASTER images per MODIS zone).

Products and algorithms

The selected emissivity products were AST_05 (ASTER) and MOD11A1 and MOD11B1 (MODIS). Acquired data were available but were still in the validation stage during our study. We used ASTER V003 data (algorithm version 2.9), which were considered as validated by the data provider, and MODIS TERRA V003 data, which were considered as provisional.[3]

AST_05 provides temperature and emissivity in ASTER bands 10–14 (**Table 1**) at a resolution of 90 m. Temperature and emissivity are retrieved using the temperature emissivity separation (TES) method developed by Gillespie et al. (1998; 1999), which combines three algorithms linked together: the normalized emissivity method (NEM), the ratio module, and the minimum maximum difference (MMD) module. NEM removes environmental radiance and gives a first guess of temperature and emissivities, assuming a maximum value for emissivities; the ratio module ratios NEM emissivities to their average; and MMD allows absolute emissivity retrieval using an empirical relationship to predict the minimum emissivity (ε_{min}). Note that the ASTER data processing depends on the spectral emissivity contrast for each pixel. The TES algorithm may not use the MMD module for low emissivity contrast (Gillespie et al., 1999).

The MOD11A1 product (**Figure 2a**) provides temperature and emissivity at a resolution of 1 km in MODIS bands 31 and 32 (**Table 1**). Temperature and emissivity are estimated using the classification-based emissivity method proposed by Snyder et al. (1998). During MODIS radiance image processing, each pixel is associated with an emissivity class mainly according to its land coverage (determined by another MODIS product) and to the year period. A look-up table with 14 emissivity classes was established by algorithm designers using reflectance models, taking into account the surface structure and for which coefficients are derived from laboratory emissivity spectra (e.g., Salisbury and D'Aria, 1992b; 1994). This emissivity information is an input for a surface temperature retrieval module called the generalized split window algorithm (Wan and Dozier, 1996; Wan, 1999). It should be noted that MOD11A1 emissivity is not a measured result, as the observed TIR radiances were not used to obtain it.

Table 1. MODIS and ASTER bands in MWIR and LWIR.

MODIS		ASTER	
Band	Limits (μm)	Band	Limits (μm)
MWIR			
20	3.660–3.840		
22	3.929–3.989		
23	4.020–4.080		
LWIR			
		10	8.125–8.475
29	8.400–8.700	11	8.475–8.825
		12	8.925–9.275
		13	10.250–10.950
31	10.780–11.280	14	10.950–11.650
32	11.770–12.270		

The MOD11B1 product (**Figure 2b**) provides temperature and emissivity in MODIS bands 20, 22, 23, 29, 31, and 32 (**Table 1**) at a resolution of 5 km using the day–night land surface temperature algorithm (Wan and Li, 1997; Wan, 1999). This algorithm allows the simultaneous retrieval of temperature and emissivity by the least-squares fit method. In this method, night and day measurements of the same surface in seven[4] bands provide enough information to solve the problem and to

[3] V004 validated MODIS emissivity collection started in February 2003 and reprocessed 2000–2002 data are now available.

[4] MODIS band 33 is used in the algorithm (Wan, 1999, p. 19) for adjusting the atmospheric variables, but emissivity in band 33 is no longer retrieved owing to the weak contribution of the surface signal in this band (Z. Wan, personal communication, 2003).

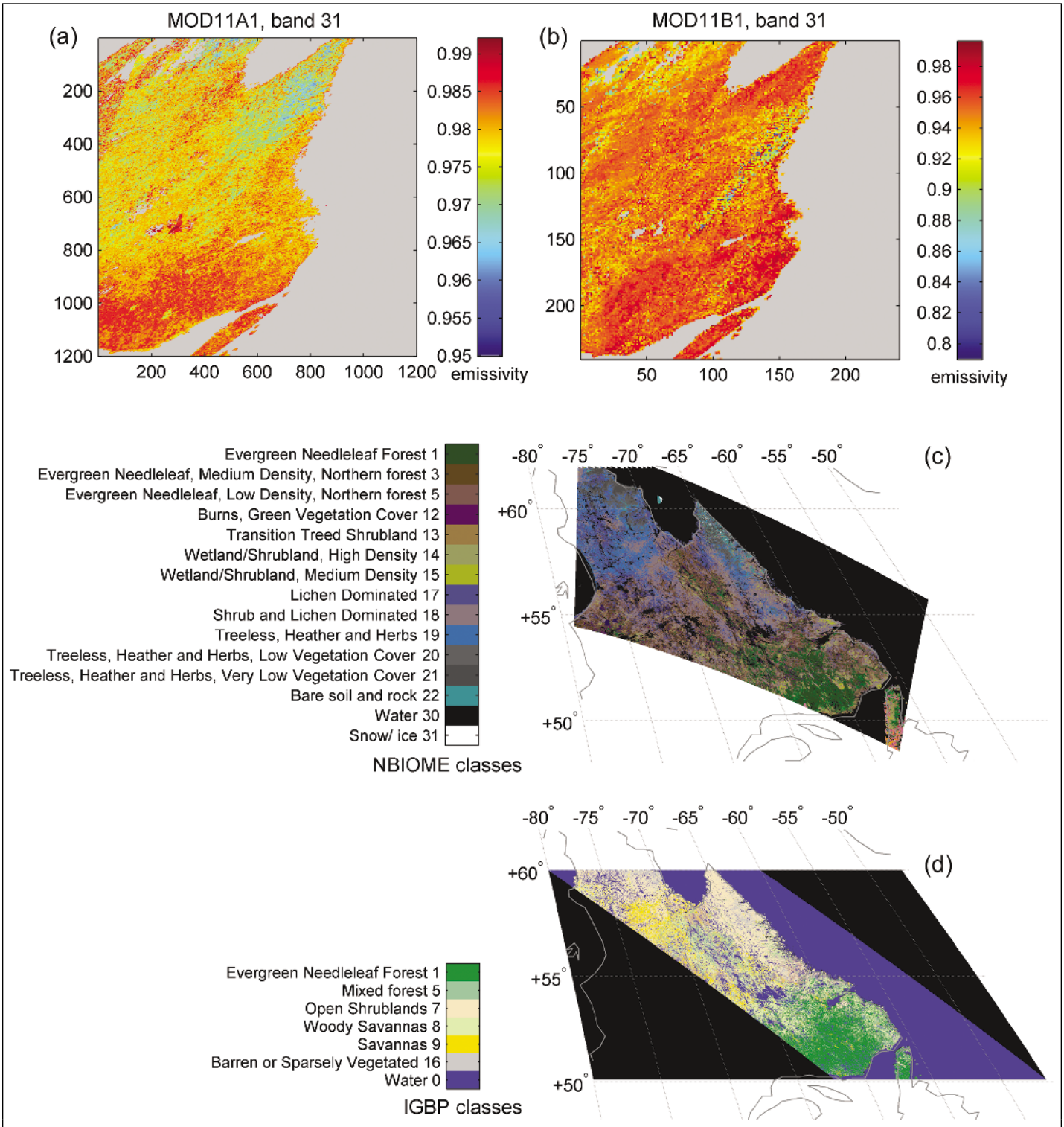

Figure 2. MOD11A1 (a) and MOD11B1 (b) data over Labrador and northern Quebec (L–NQ) for 31 July 2001. Land cover classification with the NBIOME scheme for 1995 (c) and the IGBP scheme for the period 15 October 2000 to 15 October 2001 (d) over the same area. Descriptions in the legends only list the classes found in the image.

express emissivity, night and day temperatures, and atmospheric variables.

To characterize the land cover of our zones, we used the MODIS MOD12Q1 product (1 km resolution; Strahler et al., 1999) and particularly the International Geosphere–Biosphere Programme (IGBP) data and information system classification scheme. **Figures 2c** and **2d** show the Labrador – northern Quebec zone by comparing the IGBP scheme and the classification from advanced very high resolution radiometer

images developed for the northern biome experiment (NBIOME) (Cihlar et al., 2001).

ASTER images are in Universal Transverse Mercator (UTM) projection covering a 60 km × 60 km region, and MODIS images are in integerized sinusoidal projection (ISIN grid)[5] (Masuoka et al., 1998) covering an area of about 1200 km × 1200 km. Moreover, it should be noted that viewing angles in ASTER and MODIS observations may be different (scanning pattern of ±8.55° for ASTER in TIR and ±55° for MODIS).

Methodology

A multiscale comparison was made between ASTER and MODIS emissivity images for the same geographical zone and the same date. To solve the scaling issue, we chose to average emissivity to express it at a coarser resolution (Chehbouni et al., 1995; Coret et al., 2001).

The following process was similarly applied on MOD11A1 (1 km) and MOD11B1 (5 km) images. The MODIS image was cropped to fit the ASTER extension. Geographical coordinates were computed for each pixel in the ASTER and MODIS images. We reduced ASTER resolution by averaging all AST_05 emissivity values geographically included in each MODIS pixel, and then a pixel-to-pixel scatterplot was produced.

For the class spectral signature determination, only classes representing more than 1% of the MOD12Q1 image were considered. The AST_05 image was aggregated in the same way as described earlier. The mean ASTER emissivity spectrum was then calculated for all pixels of each individual class. For MOD11B1 class signatures, the emissivity image has a coarser resolution (5 km) than the land cover class image, but they are in the same projection and cover the same geographic area. Thus, a coarser class image was computed by determining pure 5 pixel × 5 pixel blocks (i.e., containing more than 80% of one class), and nonpure blocks were masked. A list of the classes considered and corresponding statistics are provided in **Table 2**.

Results

Comparison of emissivity products

Figure 3 shows band comparisons of emissivities given by the algorithms. Comparisons were made pixel by pixel on image couples for corresponding dates and locations, and all points were then drawn on the same graph. Root mean square error (rmse) between the two datasets is indicated on the graphs.

Figure 3 clearly shows differences in emissivity dynamic range between each algorithm. MOD11B1 dynamic range is larger than that of AST_05, which is larger than that of MOD11A1. Since MODIS band 31 overlaps ASTER bands 13 and 14 (**Table 1**), the relationship between emissivities was verified for each case. ASTER band 14 fits better with MODIS band 31, for both MOD11A1 and MOD11B1 (inferior bias and rmse in **Figures 3c** and **3d**). Moreover, **Figures 3d** and **3e** show that the MOD11B1 algorithm underestimates emissivity in comparison with AST_05 (negative bias). The comparison between MOD11A1 and MOD11B1, deduced from **Figure 3**, as they are compared with the same AST_05 data (direct comparison not shown here), shows that MOD11B1 data exhibit a larger dynamic range for emissivities than MOD11A1 data.

Although a disparity was found between product dynamics, global concordance (expressed by rmse) between emissivities retrieved by different algorithms remains in the same magnitude as the expected uncertainty for these algorithms (e.g., rmse < 0.03 for TES; Payan and Royer, 2004).

Spectral signatures from ASTER and MODIS

Figure 4 shows MODIS and ASTER spectral signatures obtained by averaging class emissivities over all images (dates and locations all mixed up). After processing, we grouped classes 1 and 5 (**Table 2**) signatures, as they were very similar.

In all cases, we notice that emissivity slightly increases with an increase in vegetation density. For MODIS in LWIR, we can only separate two land cover class groups, which mainly differ by their vegetation density (forest and taiga classes against open shrubland and barren land classes). In MWIR, all four classes are distinct in MODIS band 23. For ASTER, different

Table 2. Data description for each analysed class (see **Figure 1** for location).

IGBP class	Description	Sensor	Location	No. of images	Total no. of 5 km pixels used
1 + 5	Forest	MODIS	L–NQ, SMO	22	319 494 + 8 604
		ASTER	SMO	5	8 726 + 2 208
8	Herbaceous system + forest canopy cover 30–60% (taiga)	MODIS	L–NQ	10	6 443
7	Open shrublands (tundra)	MODIS	L–NQ, NT–NV	17	91 437
		ASTER	NT–NV	2	855
16	Barren or sparsely vegetated	MODIS	NT–NV	7	17 725
		ASTER	NT–NV	2	2 081

[5] For validated products (V004), a classic sinusoidal projection is now used.

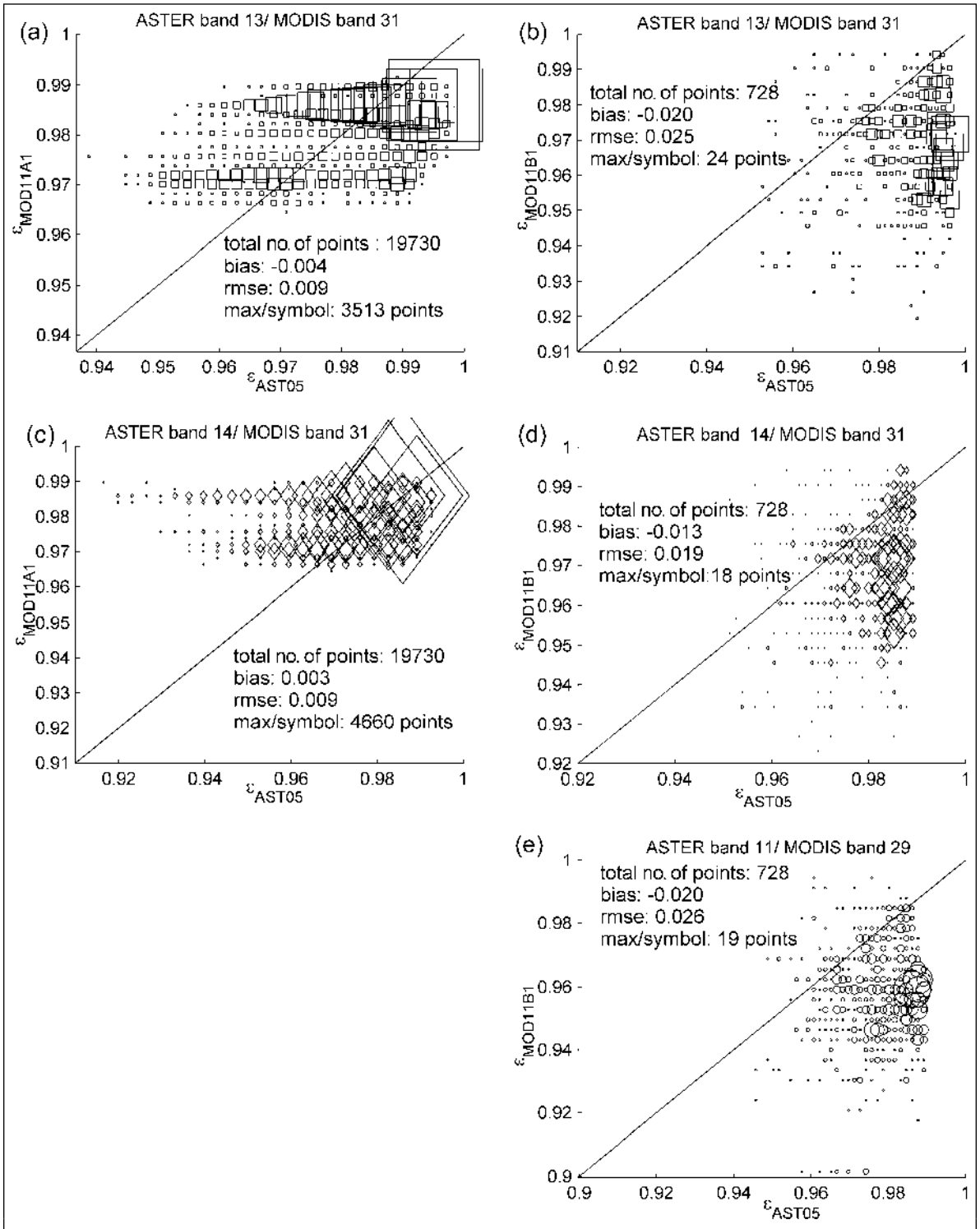

Figure 3. Emissivity (ε) band comparison from ASTER on the *X* axis (AST_05 product) and MODIS on the *Y* axis given by the MOD11A1 (a, c) and MOD11B1 (b, d, e) algorithms.The symbol size is proportional to the point density (for MOD11A1) or the square of the number of points (for MOD11B1), and the maximum number of points per symbol is indicated on the graphs. The line for $Y = X$ is plotted on each graph.

classes have similar signatures, whereas the forest class seems to be singular, especially in ASTER band 13 (10.6 µm). Moreover, we observe that ASTER emissivity values are higher than the MODIS values, e.g., MODIS band 29 (8.6 µm) gives emissivities between 0.935 and 0.950 for all classes, whereas ASTER band 11 (similar wavelengths) gives emissivities between 0.970 and 0.980. Note that in **Figure 4** we consider average emissivities by class, whereas **Figure 3** shows

a direct pixel by pixel comparison. This may explain the slight apparent difference in the average bias seen in **Figures 3** and **4** between MOD11B1 and ASTER. Lastly, the increasing emissivity trend from MODIS bands 29 and 31 is not observed between ASTER bands 11 and 14.

Spectral signature accuracy determination is not obvious. Computed standard deviations associated with means (plotted in **Figure 4**) over all images indicate reproducibility. These standard deviations are relatively small (≤0.012), indicating that the signatures are similar from one image to another. The class spatial homogeneity is another coherence criterion of our signatures. In this study, this is expressed by standard deviation over pixels used for each class characterization. For AST_05, this standard deviation over pixels is similar to the standard deviation over images, whereas for MOD11B1 the standard deviation over pixels is five times larger than that over images and is therefore greater than the distance between spectral signatures in **Figure 4**. In this study, emissivity classes are not spatially homogeneous, especially in the case of MODIS. It appears that emissivity, as a deterministic parameter of land cover types, could contain other information not considered in land cover classification criteria.

Conclusions

Although comparisons between emissivity values of the different algorithms were achieved, disparities in emissivity dynamics were identified. Moreover, direct comparison of MOD11B1 and AST_05 products, as emissivity spectra analysis, could lead one to suppose that the day–night algorithm underestimates emissivity in comparison with TES. There are several possible causes that could explain the results we found, namely, differences in atmospheric correction methods, the change of spatial scale and viewing angle introduced for the comparison, or the different meaning of retrieved emissivity according to each algorithm. Petitcolin et al. (2002) also compared TES and the two MODIS methods with another algorithm called the temperature-independent spectral index (TISI; Becker and Li, 1990) applied to raw MODIS data over arid regions, and they also observed range differences between MOD11B1 and TISI results.

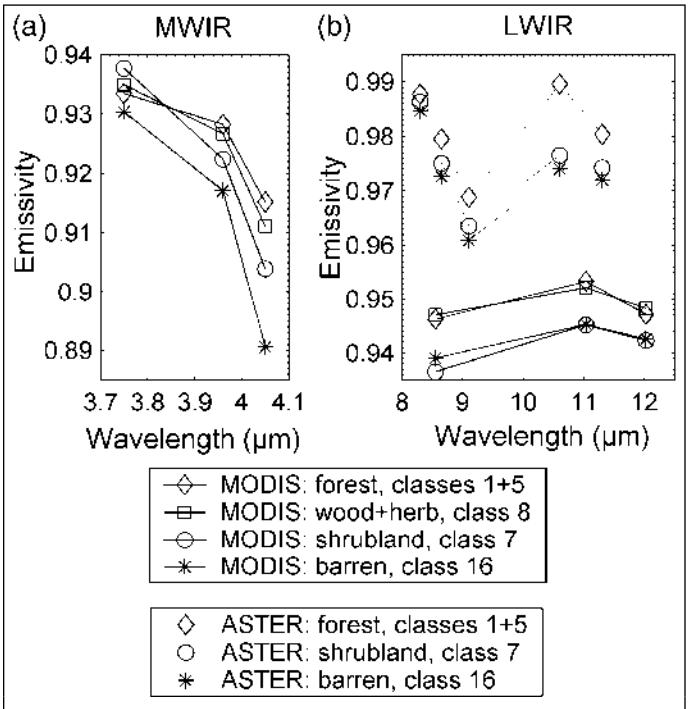

Figure 4. Comparison between spectral emissivity by class (see **Table 2**) derived from AST_05 and MOD11B1 data in MWIR (a) and LWIR (b).

Concerning emissivity spectra of land cover types, numerous studies (e.g., Salisbury and D'Aria, 1992a; 1992b; 1994) show that emissivity signatures identify surfaces at least from ground measurements. There is no doubt that vegetation gives higher emissivities than bare soil and that vegetation signatures are more monotonic than strongly featured soil spectra. Snyder et al. (1998) used emissivity classes in MODIS bands 31 and 32 for the classification-based algorithm, and Petitcolin and Vermote (2002) applied TISIE (a modified TISI) to arid zones and retrieved realistic bare soil and vegetation spectral signatures. Meanwhile, surface characterization from satellite measurements seems to be more problematic. Our attempt to define northern land cover spectral signatures gives no evident results, as class differentiation is questionable and emissivity spatial variability for a class could not be neglected. We suggest investigating if other vegetation indicators such as the leaf area index could help in defining classes with emissivity. Also, spectral unmixing could give interesting results on ASTER and MODIS emissivity data and deserves further investigation.

We have highlighted the difficulty of emissivity surface characterization in the infrared domain and we raise the question of what does emissivity represent at a global scale. In addition, we are fully aware that our data were not completely validated for our study. Nevertheless, our work could be considered as a preliminary step in testing the reliability and coherence of these algorithms, and we believe that our results are encouraging when considering the early stage of research in emissivity satellite imagery.

Acknowledgements

This work was cofunded by the Natural Sciences and Engineering Research Council of Canada (NSERC). The authors would especially like to thank François Petitcolin for helpful comments and gratefully acknowledge the MODIS team (Zhengming Wan and Zhao Liang Li) for providing the MODIS data.

References

Becker, F., and Li, Z.L. 1990. Temperature-independant spectral indices in thermal infrared bands. *Remote Sensing of Environment*, Vol. 32, pp. 17–33.

Chehbouni, G., Njoku, E.G., Lhomme, J.P., and Kerr, Y.H. 1995. Approaches for averaging surface parameters and fluxes over heterogeneous terrain. *Journal of Climate*, Vol. 8, pp. 1386–1393.

Cihlar, J., Beaubien, J., and Park, B. 2001. *BOREAS follow-on DSP-01 NBIOM level-4 AVHRR land cover, Canada, version 1.1, 1995* [online]. Available from http://www.daac.ornl.gov (Oak Ridge National Laboratory Distributed Active Archive Center, Oak Ridge, Tenn.) [cited 2002].

Coret, L., Briottet, X., Kerr, Y.H., and Chehbouni, G. 2001. Change of spatial scale over heterogeneous surface in thermal infrared remote sensing. In *Proceedings of the 8th International Symposium on Physical Measurements and Signatures in Remote Sensing*, 8–12 Jan. 2001, Aussois, France. Centre National d'Études Spatiale (CNES), Paris. pp. 91–98.

Dash, P., Göttsche, F.-M., Olesen, F.-S., and Fischer, H. 2002. Land surface temperature and emissivity estimation from passive sensor data: theory and practice — current trends. *International Journal of Remote Sensing*, Vol. 23, No. 13, pp. 2563–2594.

Gillespie, A.R., Rokugawa, S., Matsunaga, T., Cothern, J.S., Hook, S., and Kahle, A.B. 1998. A temperature and emissivity separation algorithm for advanced spaceborne thermal emission and reflection radiometer (ASTER) images. *IEEE Transactions on Geoscience and Remote Sensing*, Vol. 36, No. 4, pp. 1113–1126.

Gillespie, A.R., Rokugawa, S., Hook, S., Matsunaga, T., and Kahle, A.B. 1999. *Temperature/emissivity separation algorithm theoretical basis document (ATBD version 2.4)* [online]. Available from http://www.science.aster.ersdac.or.jp/en/documnts/pdf/2b0304.pdf [cited 2003].

Justice, C.O., Vermote, E., Townshend, J.R.G., Defries, R., Roy, D.P., Hall, D.K., Salomonson, V.V., Privette, J.L., Riggs, G., Strahler, A., Lucht, W., Myneni, R., Knyazikhin, Y., Running, S., Nemani, R.R., Wan, Z., Huete, A.R., van Leeuwen, W., Wolfe, R.E., Giglio, L., Muller, J.P., Lewis, P., and Barnsley, M.J. 1998. The moderate resolution imaging spectroradiometer (MODIS): land remote sensing for global change research. *IEEE Transactions on Geoscience and Remote Sensing*, Vol. 36, No. 4, pp. 1228–1249.

Masuoka, E., Fleig, A., Wolfe, R.E., and Patt, F. 1998. Key characteristics for MODIS data products. *IEEE Transactions on Geoscience and Remote Sensing*, Vol. 36, No. 4, pp. 1313–1323.

Payan, V., and Royer, A. 2004. Analysis of temperature emissivity separation (TES) algorithm applicability and sensitivity. *International Journal of Remote Sensing*, Vol. 25, No. 1, pp. 15–37.

Petitcolin, F., and Vermote, E. 2002. Land surface reflectance, emissivity and temperature from MODIS middle and thermal infrared data. *Remote Sensing of Environment*, Vol. 83, pp. 112–134.

Petitcolin, F., Nerry, F., and Stoll, M.P. 2002. Mapping temperature independent spectral indices of emissivity and directional emissivity in AVHRR channels 4 and 5. *International Journal of Remote Sensing*, Vol. 23, No. 17, pp. 3473–3491.

Salisbury, J.W., and D'Aria, D.M. 1992a. Infrared (8–14 μm) remote sensing of soil particle size. *Remote Sensing of Environment*, Vol. 42, pp. 157–165.

Salisbury, J.W., and D'Aria, D.M. 1992b. Emissivity of terrestrial materials in the 8–14 μm atmospheric window. *Remote Sensing of Environment*, Vol. 42, pp. 83–106.

Salisbury, J.W., and D'Aria, D.M. 1994. Emissivity of terrestrial materials in the 3–5 μm atmospheric window. *Remote Sensing of Environment*, Vol. 47, pp. 345–361.

Smith, S.L., and Burgess, M.M. 1999. Mapping the sensitivity of Canadian permafrost to climate warming. In *Interactions between the cryosphere, climate, and greenhouse gases*. Edited by M. Tranter, R. Armstrong, E. Brun, G. Jones, M. Sharp, and M. Williams. International Association of Hydrological Sciences (IAHS) Press, Wallingford, U.K., IAHS Publication 256, pp. 71–81.

Snyder, W.C., and Wan, Z. 1998. Classification-based emissivity for land surface temperature measurement from space. *International Journal of Remote Sensing*, Vol. 19, No. 14, pp. 2753–2774.

Strahler, A., Muchoney, D., Friedl, M., Gopal, S., Lambin, E., and Moody, A. 1999. *MODIS land cover and land cover changes algorithm theoretical basis document (ATBD version 5.0.)* [online]. Available from http://modis.gsfc.nasa.gov/data/atbd/atbd_mod12.pdf [cited 2003].

Wan, Z. 1999. *MODIS land-surface temperature algorithm theoretical basis document (LST ATBD version 3.3)* [online]. Available from http://modis.gsfc.nasa.gov/data/atbd/atbd_mod11.pdf [cited 2003].

Wan, Z., and Dozier, J. 1996. A generalized split-window algorithm for retrieving land-surface temperature from space. *IEEE Transactions on Geoscience and Remote Sensing*, Vol. 34, No. 4, pp. 892–905.

Wan, Z., and Li, Z.L. 1997. A physics-based algorithm for retrieving land-surface emissivity and temperature from EOS/MODIS data. *IEEE Transactions on Geoscience and Remote Sensing*, Vol. 35, No. 4, pp. 980–996.

Yamaguchi, Y., Kahle, A.B., Tsu, H., Kawakami, T., and Pniel, M. 1998. Overview of advanced spaceborne thermal emission and reflection radiometer (ASTER). *IEEE Transactions on Geoscience and Remote Sensing*, Vol. 36, No. 4, pp. 1062–1071.